University of Arkansas, Fayetteville
ScholarWorks@UARK

Electrical Engineering Undergraduate Honors Theses | Electrical Engineering

5-2019

# Modeling Solder Ball Array Interconnects for Power Module Optimization

Paul Swearingen

Follow this and additional works at: https://scholarworks.uark.edu/eleguht

Part of the Electrical and Electronics Commons, and the Power and Energy Commons

Recommended Citation
Swearingen, Paul, "Modeling Solder Ball Array Interconnects for Power Module Optimization" (2019). *Electrical Engineering Undergraduate Honors Theses*. 65.
https://scholarworks.uark.edu/eleguht/65

This Thesis is brought to you for free and open access by the Electrical Engineering at ScholarWorks@UARK. It has been accepted for inclusion in Electrical Engineering Undergraduate Honors Theses by an authorized administrator of ScholarWorks@UARK. For more information, please contact ccmiddle@uark.edu.

# Modeling Solder Ball Array Interconnects for Power Module Optimization

Paul R. Swearingen

Student ID No. 010243485

University of Arkansas

April 2019

# Table of Contents

Table of Figures ..... 3
Table of Tables ..... 3
Originality ..... 4
Acknowledgment ..... 4
I. INTRODUCTION ..... 5
II. Solder Ball Self-Inductance ..... 7
A. Geometric Characterization ..... 8
B. Solder Geometry Calculation ..... 8
C. Self-Inductance Formula ..... 10
D. Calculations Using Formula ..... 10
E. 3D Solder Ball Modeling ..... 11
F. Simulation Parameters and Results ..... 13
G. Comparison of Results ..... 13
III. Complex Impedance Due to the Skin Effect ..... 14
IV. SBA Total Inductance ..... 18
A. Mutual Inductance Formula ..... 18
B. Total Inductance Formula ..... 19
C. Calculations Using Formulas ..... 21
D. 3D SBA Modeling ..... 21
E. Simulation Parameters and Results ..... 22
F. Comparison of Results ..... 23
V. SBA Experiment ..... 23
A. Experimental Procedure ..... 23
B. Design and Fabrication Procedure ..... 24
C. Measurement Procedure ..... 27
D. Software-based Data Extraction ..... 29
1) Create Equivalent Fixture Models ..... 30
2) Refine the Model Material Parameters ..... 31
3) Convert one-port validated model to two-port through model ..... 32
4) De-embed the SBA S-parameters ..... 33
5) Convert SBA S-parameters to impedance ..... 33
E. Discussion of Experimental Results ..... 35
VI. Future Work ..... 38
VII. Conclusions ..... 39
VIII. References ..... 40

## TABLE OF FIGURES

Figure 1. Geometry determines current density of (a) solder balls and (b) wire bonds. .................................7
Figure 2. Reflowed solder ball is defined by geometric parameters. .............................................................7
Figure 3. Self-inductance of cylindrical wire is a function of height and radius. .........................................11
Figure 4. 3D Models of reflowed solder balls of 12 mil height are truncated spheres.. ...............................12
Figure 5. Self-inductance of cylindrical wires and spherical solder balls converges. .................................12
Figure 6. Resistance comparison of skin effect model with ANSYS Q3D analysis. ....................................16
Figure 7. Inductance comparison of skin effect model with ANSYS Q3D analysis and DC values. ............17
Figure 8. A comparison of skin effect inductance model results. ................................................................17
Figure 9. SBA inductance network representation for array of N solder balls. . ..........................................19
Figure 10. 3D model of a 9-interconnect SBA created in Solidworks and simulated in ANSYS Q3D. .......21
Figure 11. Total inductance is dependent on distance in a 3 x 3 Array.. .......................................................22
Figure 12. PCB created for test fixutre of 2X2 SBA. .....................................................................................24
Figure 13. Process of applying solder mask to test fixture ...........................................................................25
Figure 14. SMA ground is soldered to ground plane. .....................................................................................26
Figure 15. SMA probe is clipped and soldered. ..............................................................................................26
Figure 16. Solder balls are reflowed to open test fixture pad. ........................................................................26
Figure 17. Solder balls are reflowed between two test fixtures creating a through load. ............................26
Figure 18. Open test fixture (Setup A) is measured by VNA. .........................................................................29
Figure 19. Through-load test fixture (Setup B) is measured by VNA. ...........................................................29
Figure 20. One-port open test fixture is modeled using ADS. ........................................................................30
Figure 21. ADS model parameters are tuned to emulate measured data. ......................................................31
Figure 22. Percent error between model and measured S-parameters' real and imaginary parts. .................32
Figure 23. An ADS model is created for a two-port equivalent of the open test fixture. ..............................32
Figure 24. MATLAB de-embedding function extracts S-parameters of DUT. ............................................33
Figure 25. De-embedded resistance values of measurement. .........................................................................34
Figure 26. De-embedded reactance values of measurement. ..........................................................................35
Figure 27. Resistance measurement for valid frequency range. ....................................................................37
Figure 28. Inductance measurement for valid frequency range. ....................................................................38

## TABLE OF TABLES

Table 1. Simulated Total Inductance of 3x3 SBA. .........................................................................................22
Table 2. Solder Ball Geometry Parameters. ......................................................................................................37
Table 3. Comparison of Calculation, Simulation, and Measurement for a 4x4 Sba. ....................................37

## Originality

This project develops an accurate, low-complexity computational model for optimizing the solder ball interconnects of a power module with 3D architecture in regard to parasitic inductance. Mathematical model-based software currently exists to accommodate 2D topologies, but not 3D. Finite element analysis simulations can accomplish this task, but with significant time and computational requirements.

## Acknowledgment

P.R. Swearingen would like to thank Dr. Alan Mantooth and the University of Arkansas Packaging Group. Thanks to Andrea Wallace for assistance in familiarization of packaging topologies, software tutelage, and feedback on project progress. Thanks to Zeke Zumbro for experimental measurements and data extraction tutelage. Thanks to Paolo Vargas and Hao Chen for assistance with 3D models and simulations setup.

# Modeling Solder Ball Array Interconnects for Power Module Optimization

Paul R. Swearingen, *Member, IEEE*

*Abstract* - **PowerSynth is a software platform that can co-optimize power modules utilizing a 2D topology and wire bond interconnects. The novel 3D architectures being proposed at the University of Arkansas utilize solder ball interconnects instead of wire bonds. Therefore, they currently cannot be optimized using PowerSynth. This paper examines methods to accurately model the parasitic inductance of solder balls and ball grid arrays so they may be implemented into software for optimization. Proposed mathematical models are validated against ANSYS Electromagnetics Suite simulations. A comparison of the simulated data shows that mathematical models are well suited for implementation into optimization software platforms. Experimental measurements proved to be inconclusive and necessitate future work.**

## I. INTRODUCTION

Optimization software tools are being developed to improve electrical and thermal characteristics of wide bandgap power modules with demonstrable success. Power module loop inductances [1], thermal management, and power dissipation [2] have been modeled mathematically and by finite element analysis (FEA). One such software tool, PowerSynth, uses mathematical modeling to provide layout optimization at a rate three to four orders of magnitude more rapid than FEA [3].

One area of interest for power module optimization at the University of Arkansas is to develop alternatives to wire bond packaging techniques. They are a point of failure in thermal management of the package and contribute a non-negligible portion to the power loop inductance [4]. A solution is to utilize solder ball arrays (SBA) which are similar in form to Flip-Chip Ball Grid Arrays (FC-BGA). FC-BGAs

are 3D architectures that reduce switching distortion, on-state resistance, and power loop inductance [5] [4]. Ball grid array (BGA) packages use solder balls as interconnects in place of wire bonds. They are utilized to improve the thermal and electrical characteristics of integrated circuits usually in the form of microprocessors. Their parameters have been studied for RLC models of high frequency applications greater than 100 MHz [6], [7]. Wire bonds are the paradigm of wide bandgap power module packaging. As such, PowerSynth currently has no models for 3D architectures such as SBAs.

This paper endeavors to accurately model the parasitic inductance of solder balls and SBAs with optimization in mind. A successful model must be precise and require a reasonably small amount of computation. The mathematical models developed herein are validated against ANSYS Q3D simulations for varying solder ball geometries, diameters and arrays. Section II will replicate the self-inductance of a solder ball with a geometrically approximated formula. Section III will examine the skin effect on complex impedance. Section IV will construct a formula of the total inductance of a BGA while considering magnetic coupling between interconnects. Section V will examine the procedures and results of experimental measurements. Section VI will discuss future work for the topic. Lastly, section VII will conclude the work with discussion on implementation and other necessary validation.

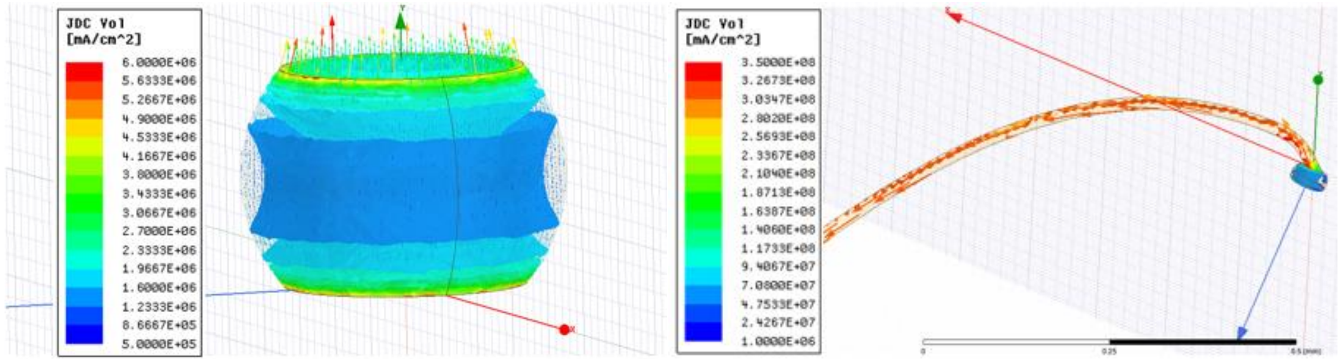


(a) (b)

***Figure 1. Geometry determines current density of (a) solder balls and (b) wire bonds.***

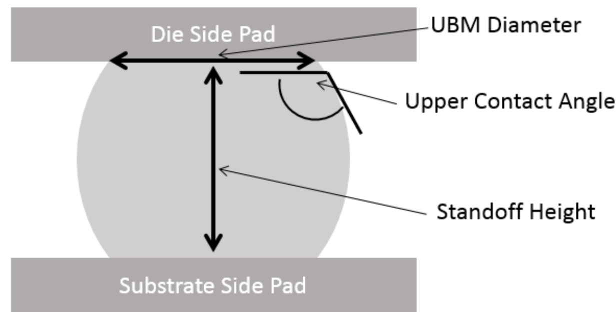


***Figure 2. Reflowed solder ball is defined by geometric parameters.***

## II. SOLDER BALL SELF-INDUCTANCE

Solder ball interconnects owe their electronic packaging advantages to their geometry. Their larger cross section and shorter length decrease current density, losses and self-inductance. Figure 1 demonstrates the two orders of magnitude reduction of current density of a solder ball (a) compared with a wire bond (b). The data was extracted from simulations performed in ANSYS Q3D software.

### *A. Geometric Characterization*

Solder balls are initially spherical pre-reflow as their name implies. Volume and reflow processes determine the standoff height, under bump metallurgy (UBM) diameter, and contact angles as seen in Fig. 2. This deformation throughout the reflow process determines fatigue life. Reference [8] demonstrates that a more acute upper contact angle and higher UBM diameter to height ratio is a more reliable geometry. This should be considered while comparing the results in Subsection F.

### *B. Solder Geometry Calculation*

Reliably predicting the geometry of a solder ball after reflow is of interest for the experimental validation of impedance models. Chiang and Yuan [9] have presented an evaluation of three solder ball shaper prediction models: truncated sphere theory, force-balanced analytical solution, and the energy-based method. Their conclusion was that all three models sufficiently replicate a reflowed solder ball's geometry. Since the simulated solder balls in this paper are modeled as truncated spheres, the truncated sphere theory will be used to compare the results of calculations, simulations and experiment.

The truncated sphere theory uses the known variables of pad radii and solder ball volume to predict the diameter and standoff height after reflow. The prediction is based on the assumption that the reflowed solder completely covers a wettable pad and does not flow past the pad boundaries. A solder ball before reflow is assumed to be spherical, so its volume is given as

$$V = \frac{4\pi * r^3}{3} \tag{1}$$

where *r* is the radius of a non-truncated sphere. After double truncation, the solder ball parameters of lower pad radius (a), upper pad radius (b), height (h), radius (R), and volume (V) are given in Eqs. (2)-(4).

$$h = \sqrt{R^2 - a^2} + \sqrt{R^2 - b^2} \tag{2}$$

$$R = \frac{\sqrt{h^4 + 2 * h^2 * (a^2 + b^2) + (a + b)^2 (a - b)^2}}{2 * h} \tag{3}$$

$$V = \frac{\pi}{12h^3} * [A(A^2 + 6a^2 * h^2) + B(B^2 + 6b^2 * h)] \tag{4}$$

where

$$A = \sqrt{h^2 + (a^2 - b^2)^2 + 2 * (b^2 - a^2) * h^2} \tag{5}$$

$$B = \sqrt{h^2 + (a^2 - b^2)^2 + 2 * (a^2 - b^2) * h^2} \tag{6}$$

For the purpose of this paper, the upper and lower pads are assumed to be the same size, a = b. This volume equation is then simplified further:

$$V = \frac{\pi * h}{6} * [h^2 + 3 * (a^2 + b^2)] \tag{7}$$

If the standoff height is known, then the radius and volume can be solved. Likewise, using Eqs. (2)-(4), radius, height and volume may be calculated if one of the three are known. These formulae are beneficial because the mathematical models discussed in this paper require the closest geometrical equivalent to a solder ball. The experimental solder ball's post-reflow, standoff height is known. Therefore, its truncated, spherical radius is also known using Eq. (3).

*C. Self-Inductance Formula*

After reflow, solder balls will vary from spherical to cylindrical geometry throughout the SBA. For this reason, it is difficult to model its self-inductance with predetermined spherical volume integrals using Eq. (8) from [10].

$$L = \frac{\mu_0}{4\pi} * \frac{1}{I^2} \iint \bar{J}_1 \cdot \bar{J}_2 \frac{d\tau_1 d\tau_2}{r_{12}} \tag{8}$$

where $\bar{J}_1$ and $\bar{J}_2$ are the current density vectors, $d\tau_1$ and $d\tau_2$ are the volume elements, and $r_{12}$ is the distance between points.

This challenge may be circumvented with a geometric approximation for a reflowed solder ball. An alternative formula is that of a straight, cylindrical wire also found in [8].

$$L = \frac{\mu_0}{2\pi} [l * \log\left(\sqrt{l^2 + R^2} + l\right) - l * \left(\log R - \frac{1}{4}\right) - \sqrt{l^2 + R^2} + 0.905415 * R] \tag{9}$$

where *log* is the natural logarithm, $l$ is the length of the wire, R is the radius, and $\mu_0$ is the permeability of free space.

*D. Calculations Using Formula*

The claim of Eq. (3)'s validity is made with the assumption that the mean final interconnect geometry will be similar to a cylinder with marginal variability. This can be verified by comparing the outputs of the formulaic model with simulation data of a 3D model over a range of radii and heights. The formula is calculated in MATLAB with radius (R) and standoff height ($l$) as independent variables. Four solder balls with heights 6, 8, 10 and 12 mils are chosen so that the effects of radius on self-inductance may be observed (Fig. 3).

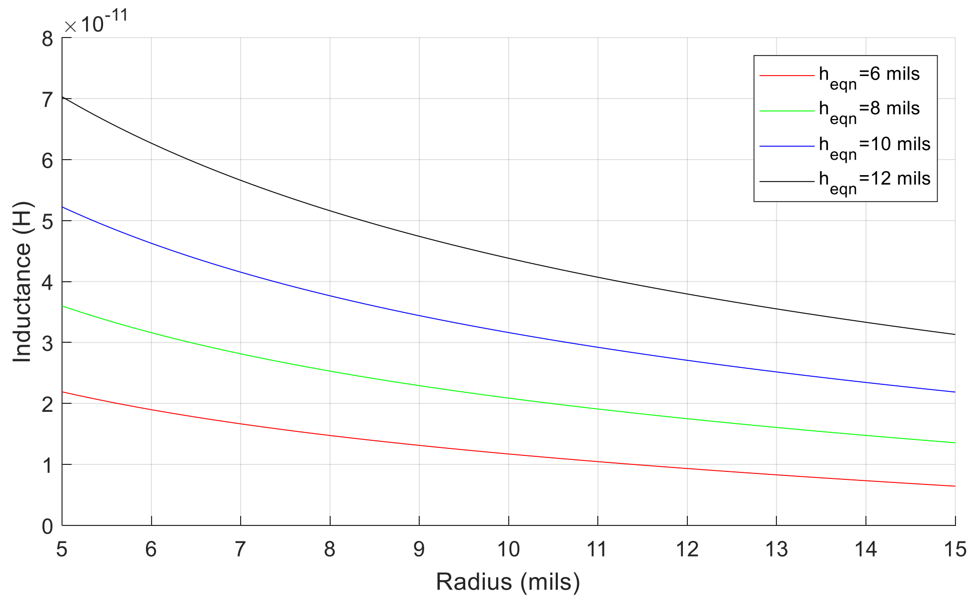


***Figure 3. Self-inductance of cylindrical wire is a function of height and radius.***

### *E. 3D Solder Ball Modeling*

The reflowed solder balls are modeled in Solidworks. The 3D models maintain a spherical geometry as height and width are varied i.e. if the radius is held constant while the height decreases, cross sections of the sphere are removed at the top and bottom of the axis to create a double truncated sphere. A solder ball with equal height and radius will more resemble a cylinder as seen in Fig. 4 (a). A solder ball with height near double the radius will be a nearly complete sphere as seen in Fig. 4 (b). Four solder balls with heights 6, 8, 10 and 12 mils are created with varying radius so that the effects of radius on self-inductance may be compared with calculated values.

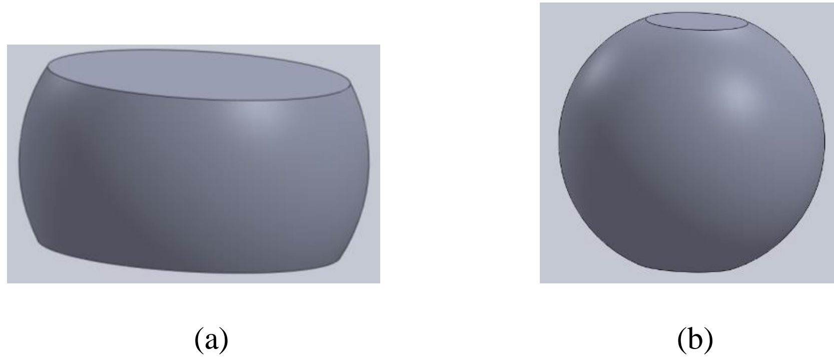


***Figure 4. 3D Models of reflowed solder balls of 12 mil height are truncated spheres. (a) 12 mil radius is cylindrical. (b) 6.5 mil radius is spherical.***

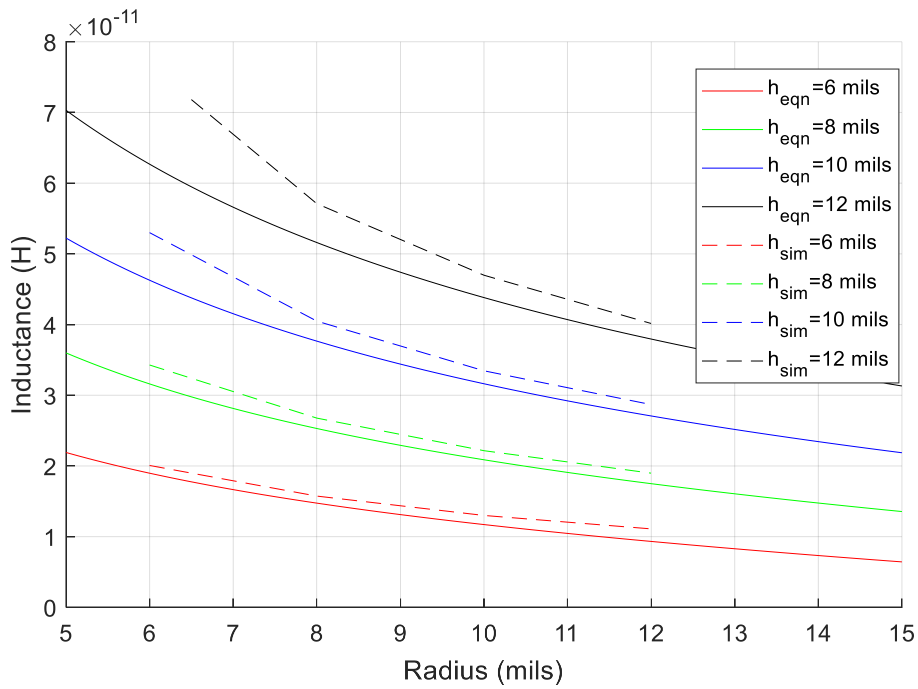


***Figure 5. Self-inductance of cylindrical wires and spherical solder balls converges with greater radius to height ratio.***

### F. Simulation Parameters and Results

The simulations are performed in ANSYS Electromagnetics Suite. The Solidworks models are imported into the Q3D Extractor and assigned to be signal nets. The flat faces are chosen to be the source and sink excitations. The solutions are set up to extract AC inductance and resistance at 500 kHz. This frequency is chosen to replicate the function of a wide bandgap power module. Each simulation completes 10 passes to refine the data. The inductance data may be applicable for frequencies up to 500 MHz as found in [11].

### G. Comparison of Results

Figure 5 presents a comparison of calculations and the simulation data. An intermediate simulation data point of 6.5 mils radius for a 12 mils height solder ball is included because a 12 mils height solder ball is a non-truncated sphere when its radius is 6 mils. No other data points are included for this radius because the solder balls are truncated at 6 mils for every other height.

There is less than 5% error for heights 6 mils and 8 mils when the radius is equal to or greater than the height. The largest divergence is seen when the height is greatest (12 mils) and the radius least (6.5 mils). This is most similar to a complete sphere, which is an undesirable geometry for a reflowed solder ball due to its larger upper contact angle [8]. In short, the mathematical model converges within 5% error of the simulated model as the solder ball sphere height decreases due to truncation. If packaging processes maintain geometries with a reasonable upper contact angle and high UBM diameter to height ratio, this formulaic model is appropriate for reliable package optimization calculations.

## III. Complex Impedance Due to the Skin Effect

Up to this point, frequency has been mostly neglected when considering the impedance of an SBA. This may not be a correct assumption as frequency becomes large. Resistance of a cylindrical wire significantly increases with frequency due to the skin effect. Inductance inversely decreases with frequency. This section focuses on developing a mathematical model to characterize the effect on impedance from frequency. The results of the model will be validated against simulations.

The basis of the model is derived by Gatous and Pissolato [12]. The work sets forth a method to find equivalent impedance by dividing the cross-section of a cylindrical conductor into $k$ circuit elements with complex impedance. The total impedance is found as a ratio of the voltage drop along the surface of the conductor to the current enclosed by it. Bessel functions are used to define the expressions for the real and imaginary parts. By solving Maxwell's wave equation, the transient formulation of the sum of the currents is obtained.

The admittance and hence the impedance is found by employing a Fourier transform and the convolution theorem. The resulting expression of admittance is

$$Y(\omega) = \sum_{k=1}^{\infty} \frac{1}{R_k + j\omega L} \tag{10}$$

where

$$R_k = \frac{\xi_k^2}{4\pi\sigma r^2} \tag{11}$$

and $\xi_k$ are the roots of the Bessel function

$$\xi_k = \frac{(2k-1)\pi}{2} + \frac{\pi}{4} \tag{12}$$

The real and imaginary parts of the admittance equation are solved for by substituting in the preceding equations to the expression for impedance Z(ω). This results in Eqs. (14) and (15), where R(ω) is resistance per meter and L(ω) is the inductance per meter of the conductor.

$$Z(\omega) = R(\omega) + j\omega L(\omega) \tag{13}$$

$$R(\omega) = \frac{\sum_{k=1}^{\infty} \frac{R_k}{{R_k}^2 + \omega^2 L^2}}{\left(\sum_{k=1}^{\infty} \frac{R_k}{{R_k}^2 + \omega^2 L^2}\right)^2 + \omega^2 \left(\sum_{k=1}^{\infty} \frac{L}{{R_k}^2 + \omega^2 L^2}\right)^2} \tag{14}$$

$$L(\omega) = \frac{\sum_{k=1}^{\infty} \frac{L}{{R_k}^2 + \omega^2 L^2}}{\left(\sum_{k=1}^{\infty} \frac{R_k}{{R_k}^2 + \omega^2 L^2}\right)^2 + \omega^2 \left(\sum_{k=1}^{\infty} \frac{L}{{R_k}^2 + \omega^2 L^2}\right)^2} \tag{15}$$

At very low frequencies, these expressions will approximate the known DC values of a resistance and inductance shown in Eqs. (16) and (17).

$$R = \frac{l}{\sigma A} \tag{16}$$

$$L = \frac{\mu l}{4\pi} \tag{17}$$

To verify the validity of the above methods, the calculated values are compared to FEA simulated values. The expressions are implemented in MATLAB. A frequency sweep simulation is conducted for a solder ball of 8 mil height and 8 mil radius in ANSYS Q3D. The sweep is conducted for 0 to 1 GHz since higher frequency validation is not necessary for the power module simulations of interest. Fig. 6 illustrates the changing resistance and Fig. 7 illustrates the changing inductance.

The resistance model appears to agree well with FEA data. The resistance expression is a suitable method for prediction and has the added benefit for executing much faster. It is also of note that the skin

effect on resistance cannot be neglected in solder balls. At the 1 MHz point, there is a 93% error between the DC resistance and the resistance from the skin effect.

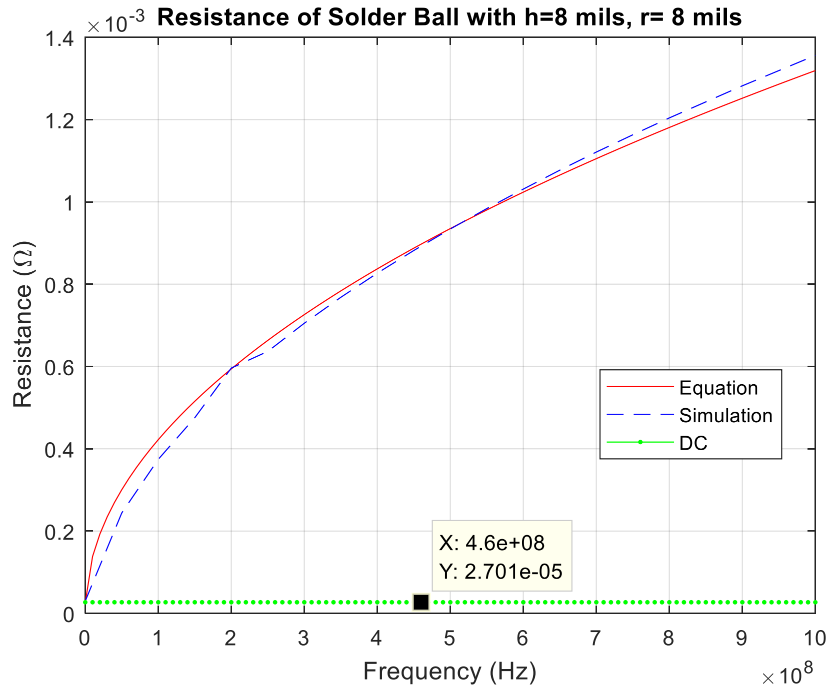


***Figure 6. Resistance from skin effect model and ANSYS Q3D analysis diverges from DC values.***

The inductance model does not appear to agree well with FEA data. While the curve of the trace follows the change in simulation values at lower frequencies, the overall values of the skin effect equation deviates by the 100 MHz point. By the 500 MHz, there is a 98% error between skin effect equations and the simulated values. This discrepancy is investigated by comparing the calculated data from this work with the inductance data from [12] (Figure 8). The log plots show similar trends, especially the 0.1 mm radius wire which is closest in size to the solder balls. According to Fig. 8 (a), the inductance decreases by approximately 3 orders of magnitude over its frequency range which is more compatible with the findings from Fig. 8 (b) and the skin effect equation trace in (**Figure** 7) This leads to the conclusion that it is not a calculation error and is instead a model error. One possibility for this model's divergence is that the inductance equation used in the Fourier expressions was for an infinitely thin wire compared to its

length. This is not the case for solder balls. Also of note is that although the self-inductance equation, Eq. (9), does not change with frequency, it remains below 5% error from the simulated values up to 1 GHz.

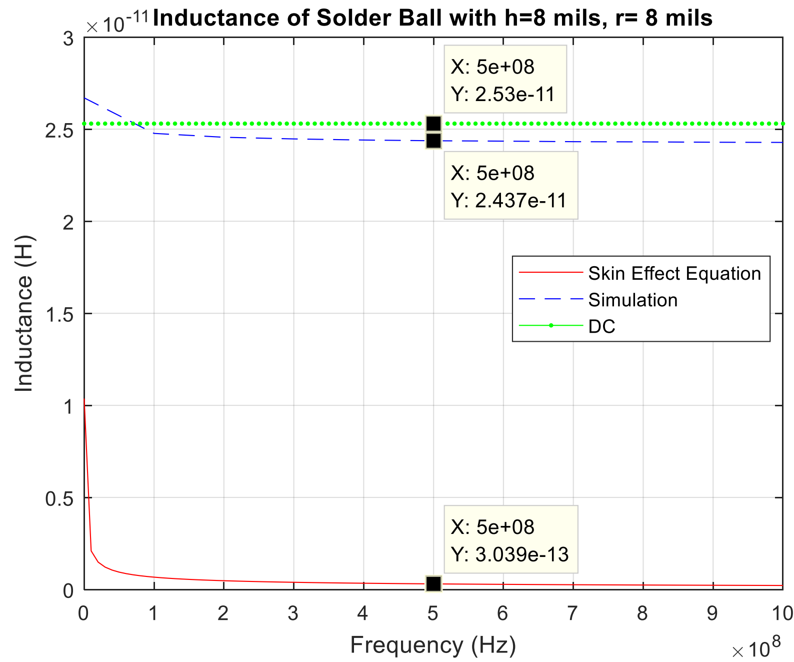


***Figure 7. Inductance comparison of skin effect model with ANSYS Q3D analysis and DC values.***

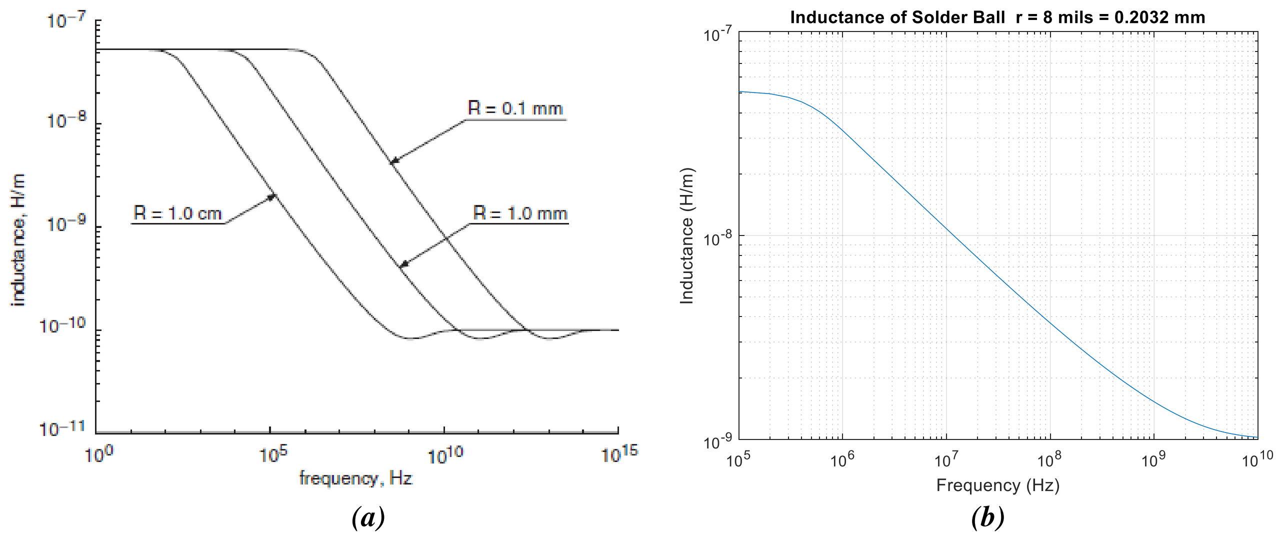


***Figure 8. A comparison of inductance model results from (a) [12] and (b) replicated calculation shows a similar decrease in magnitude over frequency.***

In summary, the expression for resistance from skin effect is validated by FEA data; however, the expression for inductance is not. One possibility for use of this information is to combine the approaches thus far. The skin effect resistance expression and Section II, Subsection C's self-inductance expression (Eqs. (9) and (14)) could be used in tandem to provide accurate data in a time and resource effective manner.

## IV. SBA TOTAL INDUCTANCE

Magnetic coupling between solder balls will also play a non-negligible role in the total inductance of a SBA. The array must be solved for parallel self-inductances along with the mutual inductance present from every solder ball coupling combination. A formulaic model for total inductance is found and compared with 3D simulations performed in ANSYS Electromagnetics Suite.

### A. *Mutual Inductance Formula*

Each solder ball of the array has a distance-dependent mutual inductance with every other solder ball. Eq. (18) is the mutual inductance formula of two cylindrical wires found in [9]. This formula is valid if both wires have the same dimensions, which is applicable for this investigation.

$$M = \frac{\mu_0}{2\pi}[l * \log(W + l) - l * \log d - W + d + \frac{R^2}{4d}] \quad (18)$$

$$W = \sqrt{l^2 + d^2 + R^2} \quad (19)$$

where *log* is the natural logarithm, $l$ is the length of the wires, $R$ is their radii, $d$ is the distance between the wire midpoints, and $\mu_0$ is the permeability of free space.

### B. *Total Inductance Formula*

The total inductance formula for the SBA neglects resistance due to the scope of this paper. **Figure** 2**Figure** 9 is a representation of the inductance network of an *N*-interconnect SBA.

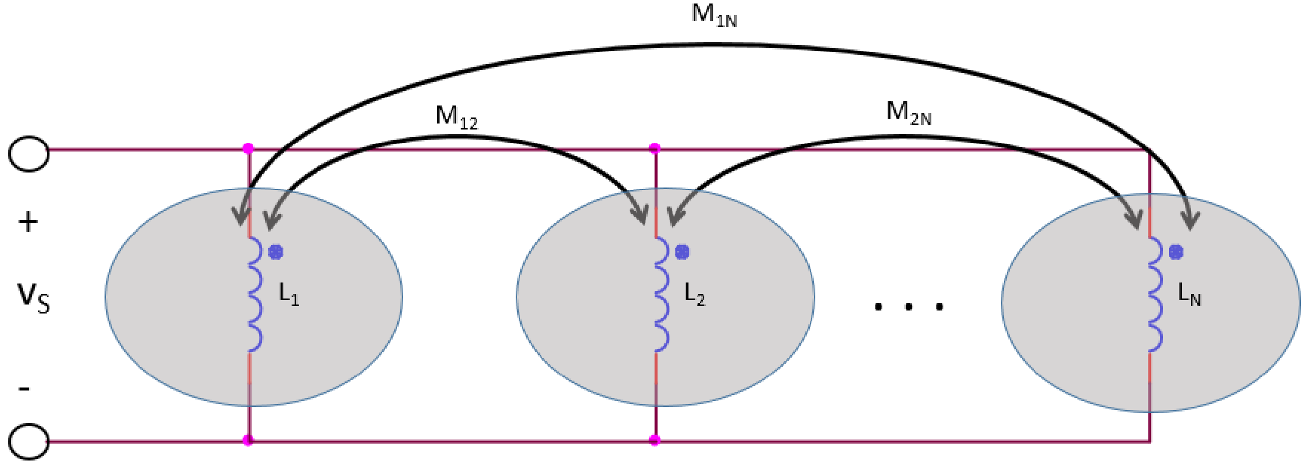


***Figure 9. SBA inductance network representation for array of N solder balls. Intermediate coupling is omitted for simplicity.***

There are *N* inductance terms for every solder ball: a self-inductance term (L) and a mutual inductance term for every other solder ball (M). With every mutual inductance value calculated, the total network inductance is solved by setting up a KVL system of equations [13].

$$v_s = L_1 \frac{di_1}{dt} + M_{12} \frac{di_2}{dt} + \cdots + M_{1N} \frac{di_N}{dt} \tag{20}$$

$$v_s = M_{12} \frac{di_1}{dt} + L_2 \frac{di_2}{dt} + \cdots + M_{2N} \frac{di_N}{dt} \tag{21}$$

$$\vdots$$

$$v_s = M_{1N} \frac{di_1}{dt} + M_{2N} \frac{di_2}{dt} + \cdots + L_N \frac{di_N}{dt} \tag{22}$$

$$\overline{v_s} = \begin{bmatrix} L_1 & M_{12} & \cdots & M_{1N} \\ M_{12} & L_2 & \cdots & M_{2N} \\ \vdots & \vdots & \ddots & \vdots \\ M_{1N} & M_{2N} & \cdots & L_N \end{bmatrix} \cdot \begin{bmatrix} \frac{di_1}{dt} \\ \frac{di_2}{dt} \\ \vdots \\ \frac{di_N}{dt} \end{bmatrix} = \overline{L}\,\overline{\frac{d\iota_{1,2,\ldots,N}}{dt}} \tag{23}$$

The system is solved in a straightforward manner with every symmetrical rectangular array. First, take the inverse of the inductance coefficient matrix, $\overline{L}$ found in equation (23). The inductance matrix is square of *N* x *N* dimension. Next, multiply both sides of the equation with the inverse as seen in Eq. (24).

$$\overline{L}^{-1}\overline{v_s} = \overline{\frac{d\iota_{1,2,\ldots,N}}{dt}} \tag{24}$$

Using KCL, the current derivatives of each branch are summed together in Eq. (25) to find the source current derivative. Performing this action on Eq. (26) is the equivalent of summing each element in the inverse of the inductance coefficient matrix. Factor $v_s$ from every matrix element and the result is Eq. (27).

$$\frac{di}{dt} = \frac{di_1}{dt} + \frac{di_2}{dt} + \cdots + \frac{di_N}{dt} \tag{25}$$

$$\left(\sum_{i=1}^{N}\sum_{j=1}^{N} L_{ij}^{-1}\right) \cdot v_s = \frac{di}{dt} \tag{26}$$

Finally, solving for $v_s$ in Eq. (27) will provide the familiar $L\frac{di}{dt}$ relationship.

$$v_s = \frac{1}{\left(\sum_{i=1}^{N}\sum_{j=1}^{N} L_{ij}^{-1}\right)} \cdot \frac{di}{dt} = L_T\frac{di}{dt} \tag{27}$$

$L_T$ may now be observed as the general Eq. (28) of total inductance for an SBA.

$$L_T = \frac{1}{\left(\sum_{i=1}^{N}\sum_{j=1}^{N} L_{ij}^{-1}\right)} \tag{28}$$

*C. Calculations Using Formulas*

All calculations are again performed in MATLAB. Once the geometry of SBA interconnects is chosen based upon design preference and reflow procedure, total inductance calculations are dependent upon interconnect amount, formation, and distance. From the results of the Section II, solder balls of 8 mil height and 8 mil radius have reasonable geometry and acceptably low percent error between formula and simulation, so they are used across all arrays. It is assumed that every array is rectangular and distance is constant between horizontally and vertically adjacent interconnects. The calculation is accomplished with nested for loops and is transferrable to any programming language. The results of a 3 x 3 array calculation is shown in Figure 11.

*D. 3D SBA Modeling*

The SBAs are modeled in Solidworks (Figure 10) and simulated in ANSYS Q3D. Distance between interconnects is the variable for this simulation of magnetic coupling. Each array holds solder ball geometry constant. As with the calculations, solder balls of 8 mil height and 8 mil radius are used across all arrays. The source and sink faces of the solder balls are connected by a plane with 0.1 µm thickness. This is the minimum thickness to model and will have the least effect on simulated inductance of the array. The plane is necessary because ANSYS Q3D must have a continuous conductor for signal net excitations.

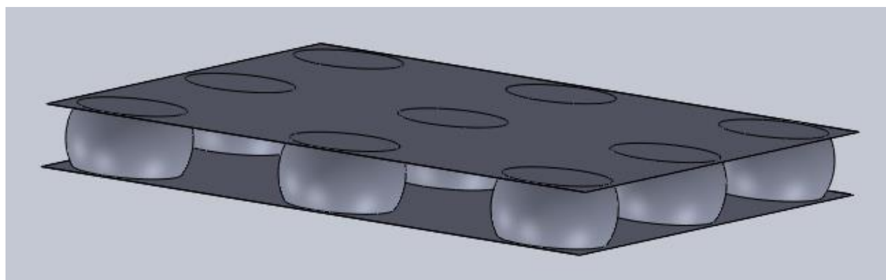

***Figure 10. 3D model of a 9-interconnect SBA is created in Solidworks and simulated in ANSYS Q3D.***

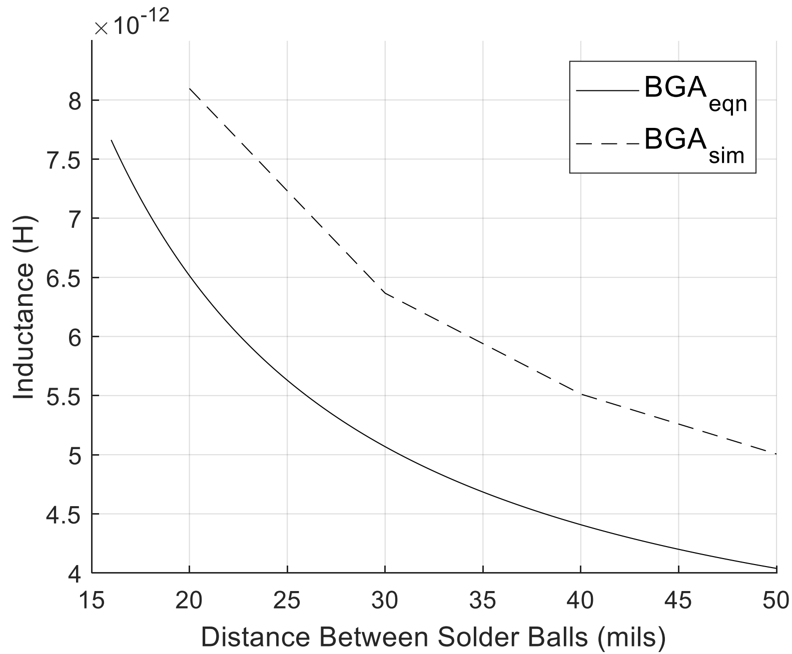


***Figure 11. Total inductance is dependent on distance in a 3 x 3 Array. This plot compares the results using the formula for an array of cylindrical wire to simulated spherical interconnects.***

***TABLE 1. SIMULATED TOTAL INDUCTANCE OF 3X3 SBA.***

| Distance (mils) | Inductance (pH) |
|---|---|
| 20 | 8.097 |
| 30 | 6.366 |
| 40 | 5.513 |
| 50 | 5.006 |

### *E. Simulation Parameters and Results*

Similar to the self-inductance simulations, the models are imported into ANSYS Q3D Extractor. The planes of the SBAs are chosen as the source and sink excitations. They are run to extract AC inductance

and resistance at 500 kHz. Each simulation completes 10 passes to refine the data. The inductance results of the simulations are shown in Table 3. The results are reasonable as a decrease in total inductance is observed with an increase in solder ball distance.

### F. *Comparison of Results*

A comparison of the simulated and calculated results is shown in Figure 11. The inductance difference between calculation and simulation for all distances of the array is less than 2 pH, which is approximately 20% error across all distances. This affirms that the mathematical model follows closely to the trend line of the simulations.

The signal planes of the simulation may exert a non-negligible influence on the coupling behavior of the interconnects. This could account for some amount of the percent error. One solution to improve the formula may be to scale it by the average percent error added to 100%. Data from the test of a real power module's parasitic parameters may inform this suggestion.

## V. SBA EXPERIMENT

### A. *Experimental Procedure*

One of the goals of this paper is to validate the preceding mathematical model and simulations against experimental data. This is accomplished by designing and fabricating an SBA test fixture, taking measurements with a vector network analyzer (VNA), and extracting impedance data from the measurements. This section will clarify the procedures of each step so that it is a repeatable process. The experimental results will be presented in the following section.

### B. *Design and Fabrication Procedure*

The strategy for designing the SBA test fixture is informed by the application of the SBA and the measurement device. The SBA under consideration is for use in flip-chip power modules. More specifically, they are the interconnects for MOSFET die. In this topology, solder mask is applied to the rectangular drain and source terminals so that each has an array cluster. For this reason, the test fixture is designed such that four solder balls are applied equidistantly to a square copper pad. The fixture must also have ports so that a measurement device may be connected. An SMA jack is chosen so that a VNA or a time domain reflectometer (TDR) may be used. Four mechanical holes allow for two fixtures to be secured together. A 12 mil micro strip line bridges the pad and connector. Finally, the bottom of the fixture is a ground plane. Fig. 12 is the fixture PCB design created in Allegro.

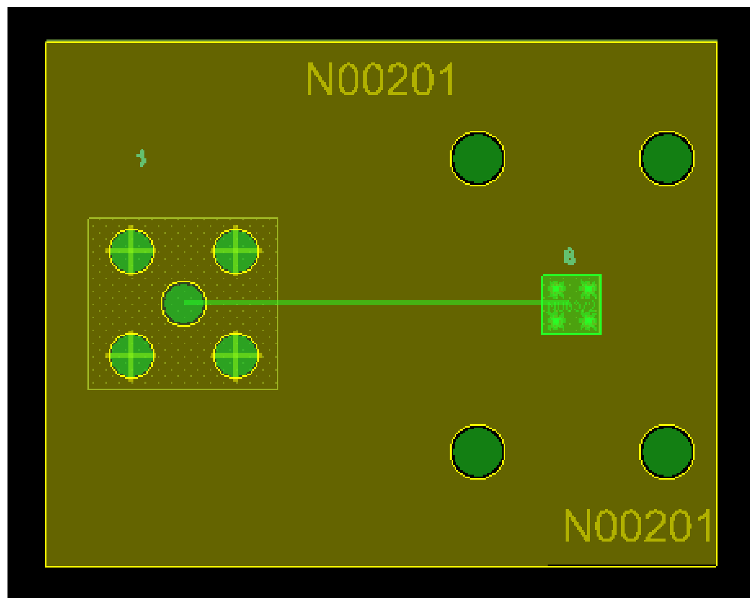


***Figure 12. PCB created for test fixutre of 2X2 SBA.***

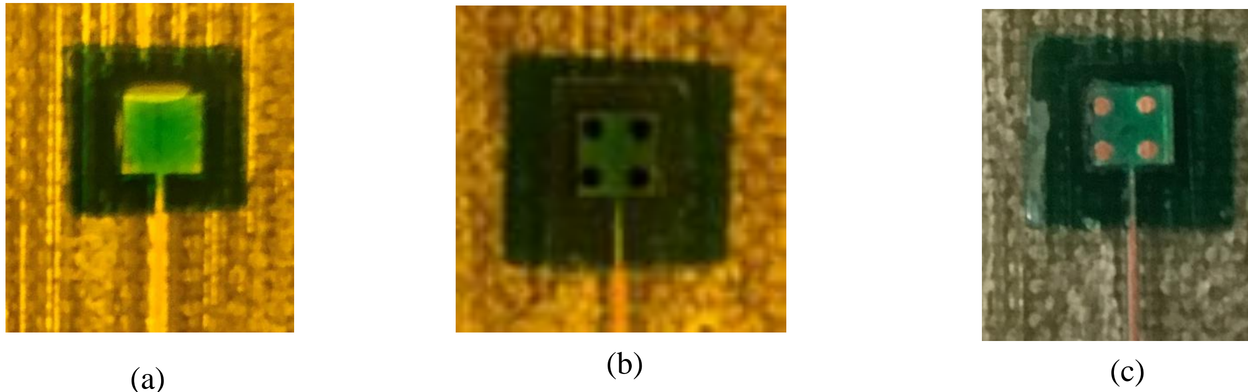
(a) (b) (c)

***Figure 13. Process of applying solder mask to test fixture consists of (a) application of mask, (b) photo mask, (c) mask with exposed holes.***

Once the PCB art and drill files have been generated, the fabrication of the fixture is accomplished by milling a substrate, applying a solder mask, reflowing the solder balls, and attaching the SMA connectors. The first step in fabricating the fixture is to use a CNC milling machine to drill an FR-4 copper cladded substrate. The top copper of the substrate should be rubbed out in locations with no essential connections. Next, a solder mask is applied to the SBA pad using photolithography. The steps for creating the solder mask are as follows:

1. Apply the solder mask. In a yellow light room, begin by cutting the solder mask to a slightly larger size than the SBA pad. Remove the Mylar and place on the top of the substrate. Use a laminator at 100 °C to laminate the substrate and solder mask (Fig. 13).
2. Place and align the photo mask on top of the solder mask.
3. Expose the substrate with the mask on it to UV light for 2.5 minutes. Remove the photo mask. Place substrate in developer solution for 5-7 minutes or until holes are open.
4. Expose the solder mask to natural light for 24 hours before soldering.

Next, the solder balls are reflowed in two steps: reflowing the solder balls to one fixture and reflowing the solder balls again to the second fixture. First, apply solder paste to the holes in the solder mask. Only apply enough to cover the exposed pad. Next, place the solder balls on top of the solder paste. Place the fixture in a reflow oven with the solder paste temperature profile. The paste should be chosen such that

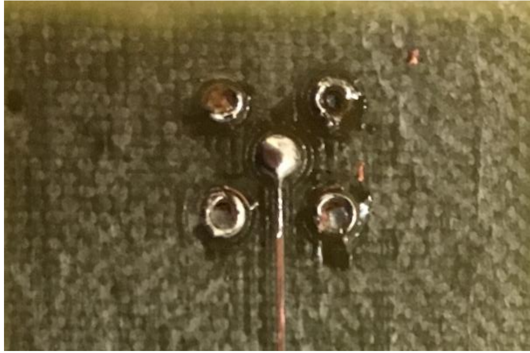

***Figure 15. SMA probe is clipped and soldered.***

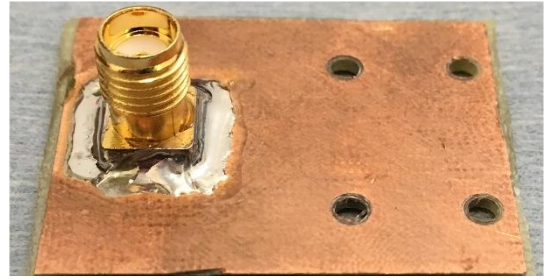

***Figure 14. SMA ground is soldered to ground plane.***

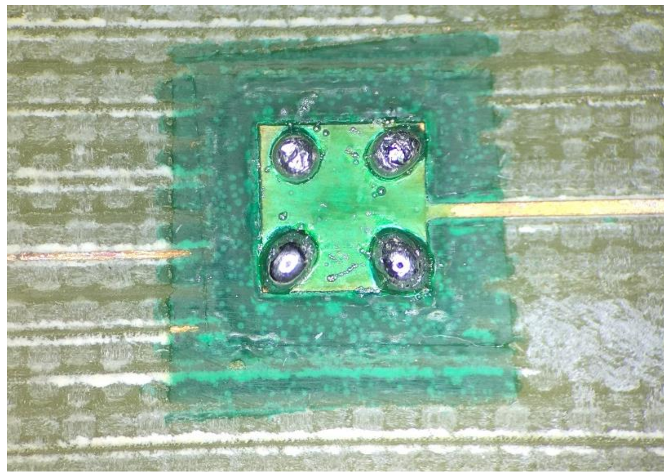

***Figure 16. Solder balls are reflowed to open test fixture pad.***

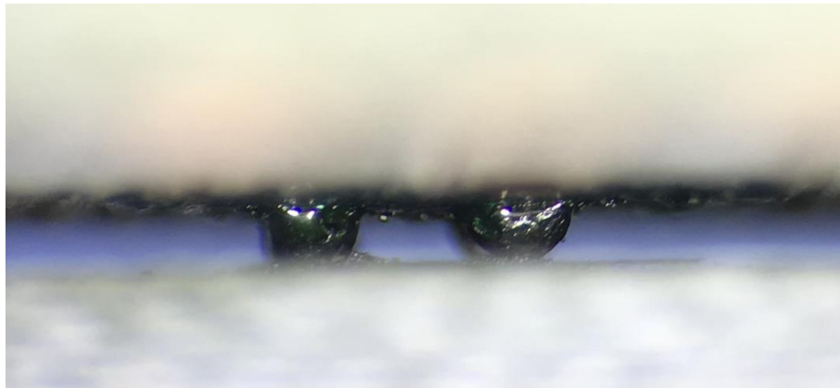

***Figure 17. Solder balls are reflowed between two test fixtures creating a through load.***

it will reflow at a lower temperature than the solder ball. Fig. 16 illustrates the outcome of reflowed solder balls. To complete the connection of the fixtures together, repeat the application of solder paste to the non-reflowed fixture. Secure the two sides together with screws and place them in the oven for a second reflow (Fig. 17).

Finally, attach the SMA connectors. Clip any extruding pins through the top side such that they are flush with the top surface. The SMA connections can be soldered with a soldering iron. Figs. 14 and 15 demonstrate the center pin and ground plane connections, respectively.

After completion of fabrication, there are two testing setups: setup A is the two fixtures attached by reflowed solder balls and setup B is a fixture with no solder balls. Having both is necessary to complete experimental measurements.

### *C. Measurement Procedure*

The two test setups will be measured using a VNA. It performs the measurements by providing a stimulus signal to a network port and tracking the response at the same port or an opposing port in the network. The amplitude and phase response are recorded and represented by the scattering, or S-parameters. Anderson [14] provides a helpful summary of these parameters. For a two-port network, there are four possible S parameter values: $S_{11}$, $S_{12}$, $S_{21}$, and $S_{22}$. $S_{11}$ is the response measured at port 1 from an excitation at port 1, also known as the input reflection coefficient. $S_{22}$ is the response measured at port 2 from an excitation at port 2, also known as the output reflection coefficient. $S_{12}$ is the response measured at port 1 from an excitation at port 2, also known as the reverse insertion gain. $S_{21}$ is the response measured at port 2 from an excitation at port 1, also known as the forward insertion gain. The mathematical representation of these parameters is

$$S_{11} = \frac{b_1}{a_1}|_{a_2=0} \tag{29}$$

$$S_{22} = \frac{b_2}{a_2}|_{a_1=0} \tag{30}$$

$$S_{21} = \frac{b_2}{a_1}|_{a_2=0} \tag{31}$$

$$S_{11} = \frac{b_1}{a_2}|_{a_1=0} \tag{32}$$

where *a* and *b* are the voltage wave incident on port *i*, also given as

$$a_i = \frac{V_i + Z_i I_i}{2\sqrt{|ReZ_i|}} \tag{33}$$

$$b_i = \frac{V_i - Z_i{}^* I_i}{2\sqrt{|ReZ_i|}} \tag{34}$$

The input impedance at port 1 can then be found by its $S_{11}$ parameters and the characteristic impedance of the network, $Z_0$

$$Z_1 = Z_0 \frac{(1 + S_{11})}{(1 - S_{11})} \tag{35}$$

The inductance values of the SBA are expected to be in the tens of picoHenrys range, so calibration is performed to de-embed the impedance of all VNA connections up to the fixtures. In calibration, attachments of short, open, load, and through are added to the VNA cables terminated by SMA connectors. Software is used to save the profiles of each calibration so that they are applied during testing. The fixtures must be de-embedded from the measurements so the SBA impedance is all that remains. Setup A is measured by its $S_{11}$ parameters for the purpose of de-embedding from the SBA setup (Figure 18). Setup B is measured using two ports so that its $S_{11}$, $S_{12}$, $S_{21}$, and $S_{22}$ parameters are extracted (Figure 19).

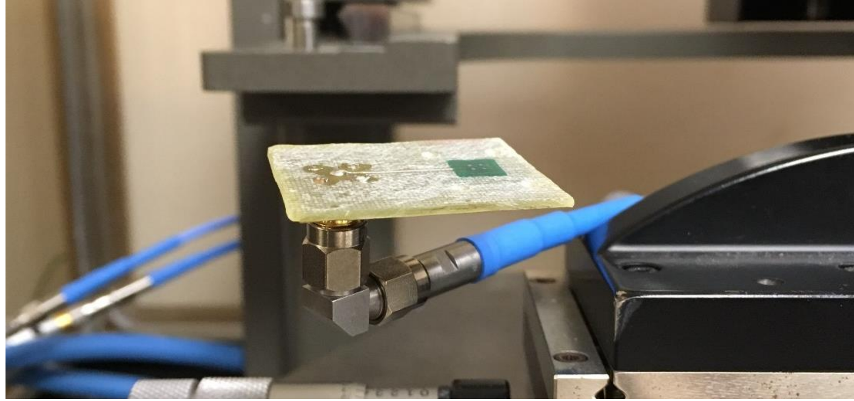

***Figure 18. Open test fixture (Setup A) is measured by VNA.***

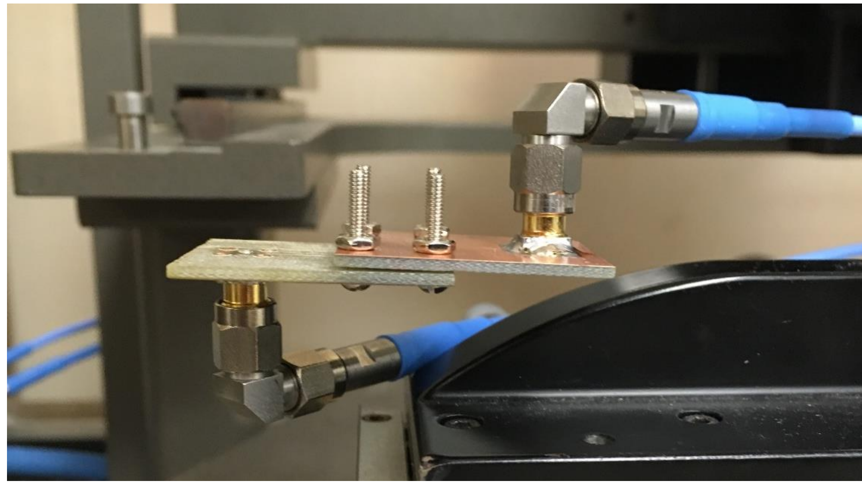

***Figure 19. Through-load test fixture (Setup B) is measured by VNA.***

*D. Software-based Data Extraction*

The data gathered from the VNA is evaluated in software for the purpose of de-embedding the test fixtures. Without de-embedding, the impedance measured with the VNA includes that from the fixture board's transmission lines. This cannot be neglected as their impedance is much greater than the impedance of the SBA. The process for impedance extraction is as follows:

1. Create equivalent fixture models in Advanced Design System (ADS).
2. Refine the model material parameters until data agrees for frequency response of a one-port measurement.
3. Convert one-port validated model to two-port through model.
4. Using two-port model, de-embed the SBA S-parameters in MATLAB.
5. Convert SBA S-parameters to impedance.

*1) Create Equivalent Fixture Models*

The test fixtures are replicated in ADS software because it provides an opportunity to extract port measurements where it may not have been feasible in an experiment. For example, the open test fixture with no SBA does not have the accessibility to conduct an $S_{12}$ or $S_{21}$ measurement. ADS can provide an equivalent circuit of the fixture as is and a theoretical port added to the opposite side. Refer to Figure 20 and 23 for the equivalent one port and two port circuits, respectively.

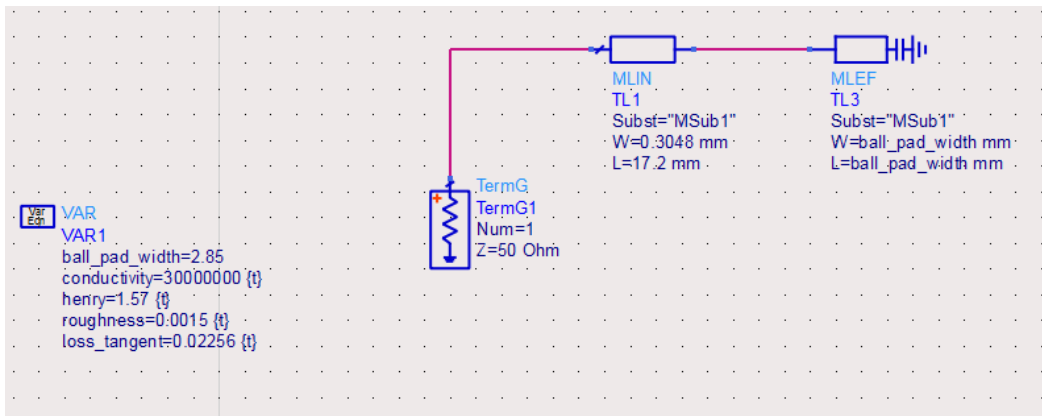


***Figure 20. One-port open test fixture is modeled using ADS.***

*2) Refine the Model Material Parameters*

The ADS equivalent circuits are only useful if they are designed to closely agree with measured data. This is accomplished by tuning the software parameters of the material. This includes conductivity, surface roughness, loss tangent, dielectric constant of the substrate, etc. Figure 21 demonstrates the most accurate one-port model derived in ADS. The simulated data appears to be valid approximately up to the 2.5 GHz range, but Figure 22 shows that the imaginary part of the S-parameters diverges beyond 10% error for frequencies above approximately 1.8 GHz. Therefore, the ADS model will be used as a de-embedding tool only for frequencies up to 1.8 GHz.

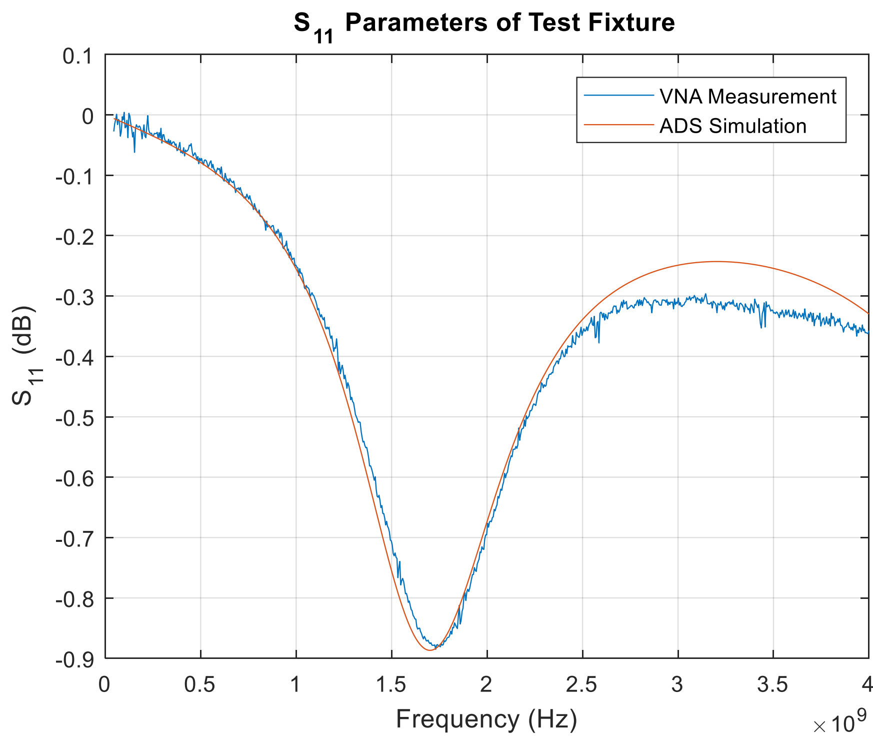


***Figure 21. ADS model parameters are tuned to emulate measured data.***

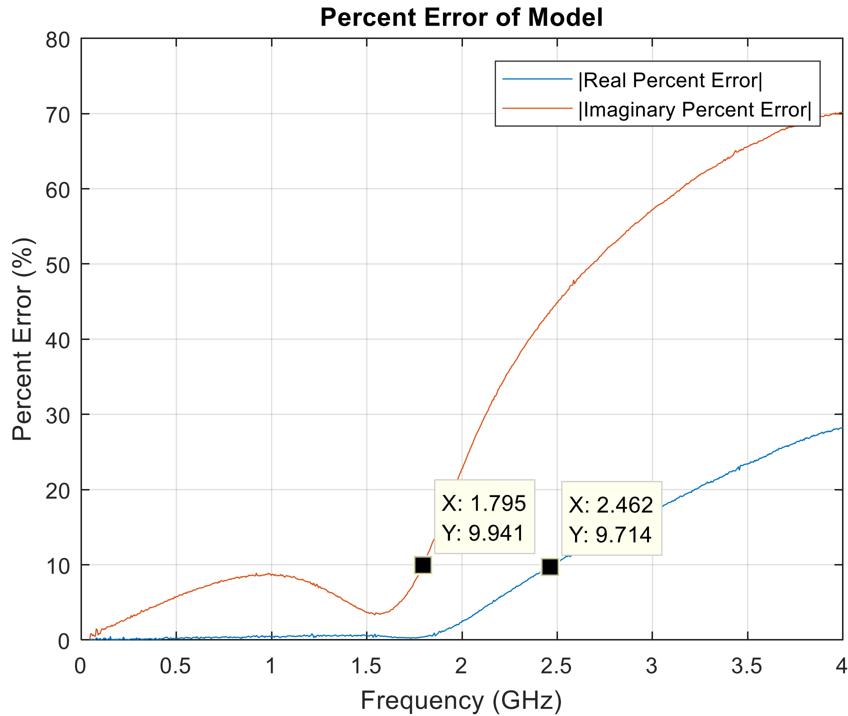


***Figure 22. Percent error between model and measured S-parameters' real and imaginary parts increases with frequency.***

*3) Convert one-port validated model to two-port through model*

$S_{21}$ and $S_{12}$ models are needed to de-embed the SBA from the test setup. The $S_{11}$ model is not sufficient because it is not through-load as in Figure 19. Subsection 2 demonstrates that the ADS fixture layout and material parameters are within 10% accuracy up to 1.8 GHz, so they are the basis for generating $S_{21}$ and $S_{12}$ parameters. This is accomplished by connecting a second port at the pad component of the model as seen in Figure 23.

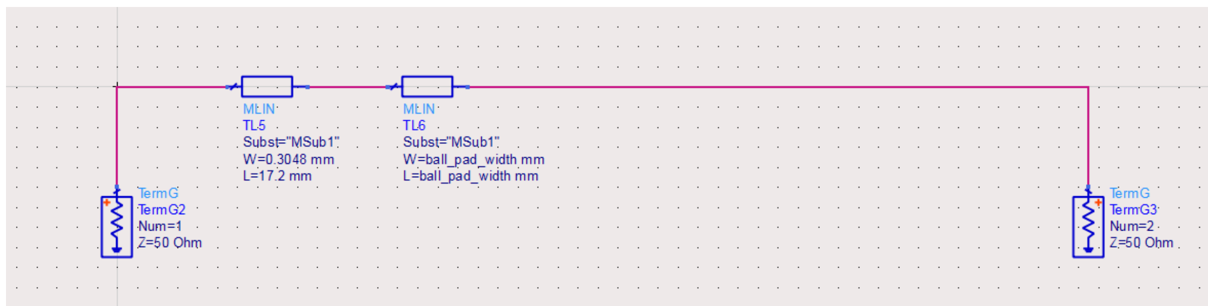


***Figure 23. An ADS model is created for a two-port equivalent of the open test fixture.***

*4) De-embed the SBA S-parameters*

After converting the one-port model to two ports in ADS, MATLAB is used to extract the model data to provide meaningful results of the SBA test structure. De-embedding the SBA S-parameters requires two MATLAB functions. First, a function to convert the open fixture model's S parameters to create the left and right side of the measured data structure seen in the $S_1$ and $S_3$ blocks in Figure 24. Second, a function to de-embed the SBA from the measured through-port data represented by block $S_2$. The "snp2smp" function effectively swaps the ports of the open-ended fixture so that the two copper pads to which the SBA is reflowed are oriented properly. The "deembedsparams" function de-embeds the two input S-parameter objects from a third overall input S-parameter object and returns the de-embedded data. In Figure 24, $S_2$ DUT represents the output data after $S_1$ and $S_3$ are de-embedded from S.

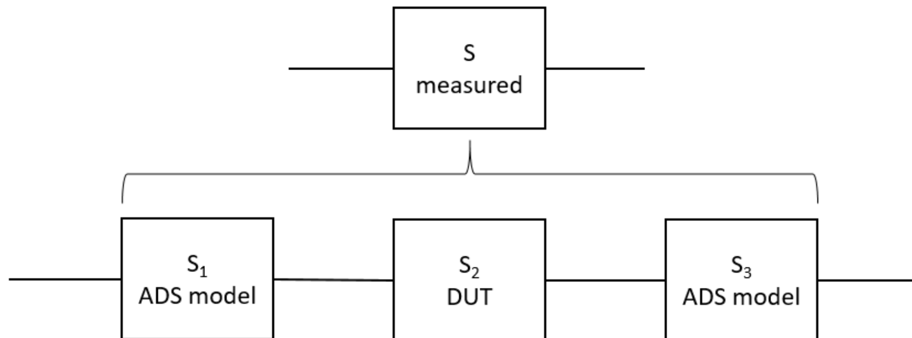


***Figure 24. MATLAB de-embedding function extracts S-parameters of DUT.***

*5) Convert SBA S-parameters to impedance*

Once the S-parameters of the DUT have been de-embedded, the SBA's S-parameters are converted to Y-parameters, also known as admittance parameters. Reveyrand and Frickey [15], [16] provide a set of formulas for this type of conversion for a multiport circuit. The MATLAB function "s2y" [17] is used to perform the conversion. This is further converted to impedance by taking the inverse. The resistance is

found by taking the real part of the array (36) and the reactance is found by taking the imaginary part and dividing by the angular frequency (38), (39).

$$R = Re\{Z\} \tag{36}$$

$$X = Im\{Z\} \tag{38}$$

$$L = \frac{X_L}{\omega} \tag{39}$$

The results of the MATLAB operations for resistance and reactance are seen in Figs. 25 and 26, respectively. A percent error graph for the ADS model vs. measurements is provided in Figure 22 to provide context for the deviance in results. This is discussed further in the following section.

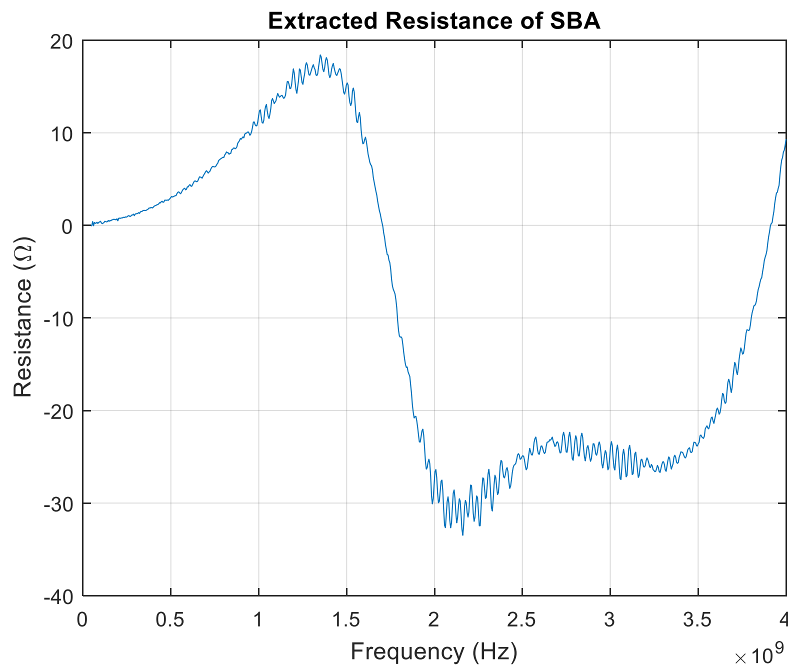


***Figure 25. De-embedded resistance values of measurement.***

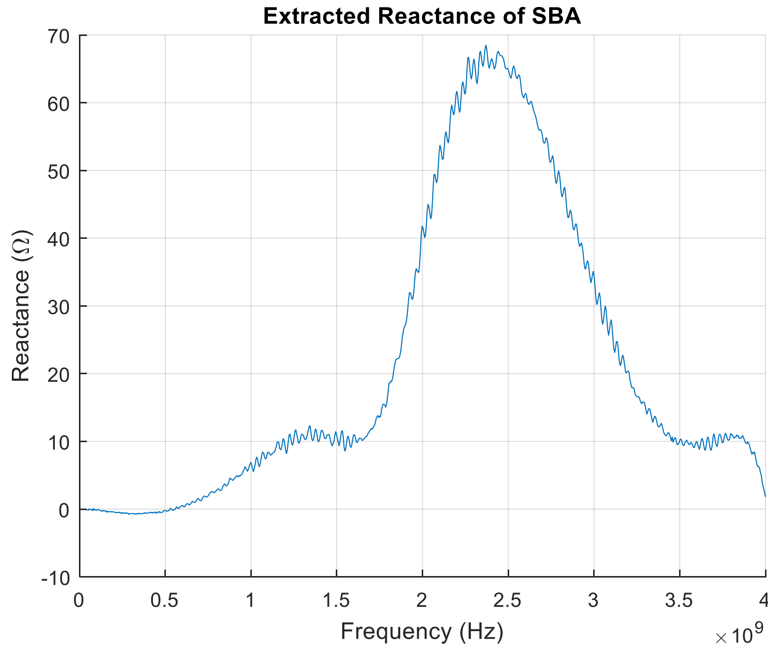


***Figure 26. De-embedded reactance values of measurement.***

## *E. Discussion of Experimental Results*

It is once again apparent that the results of de-embedding become incoherent after approximately 1.8 GHz. Figure 22 demonstrates that real impedance error between models begins to increase sharply after this point. The author asserts that it is due to the inability of the ADS model to emulate the fixture parameters after this frequency. Data under this frequency appears to have coherent and consistent results. If the data is examined more closely up to the 1.5 GHz point, trends can be seen more clearly. Figure 27 shows that there is an almost linear increase in resistance through this frequency range. This agrees with the trend found in Fig. 6 of Section III where the skin effect on solder balls was evaluated.

The extracted reactance of the DUT is less straightforward (Figure 28). At low frequencies, the reactance is negative which implies that the capacitance of the test fixture is dominating. After 600 MHz, the reactance becomes positive and the inductance plays a more prominent role in the impedance of the DUT. According to the plot, the inductance measurement reaches a maximum of approximately 1.3 nH

before the data becomes inconsistent after the 1.8 GHz point. The data is compared to SBA models built from the data calculated by equations in Section II, Subsection B. The standoff height of the fabricated SBA fixture is used to calculate the solder ball radius. The parameters to emulate the fixture are found in

TABLE 2. With these values, a mathematical and simulated model is constructed as done previously. A comparison is made between all the evaluation methods for SBA inductance in TABLE 3. The measured value is two orders of magnitude greater than the calculated and simulated results. This is a significant difference and does not correspond to the calculated and measured results.

It is the author's assertion that the test fixture of the SBA is imperfect and in need of refinement. There are several possible explanations as to why there is significant deviation in the experimental values that do not invalidate the proposed evaluation methods. One possibility is that the test fixtures have different impedances due to inconsistencies in fabrication. These inconsistencies include variation in trace width and solder connections of the SMA connector. It is recommended that $S_{11}$ measurements be taken of all fixtures of the SBA test structure before they are reflowed together by the solder balls. It is an error that this was not done for this experiment. Another possibility is the signal to the tested SBA created unforeseen parasitic effects due to its directional nature. That is to say, the excitation from the VNA was perpendicular to the solder balls, whereas the ANSYS Q3D simulation assumed a parallel excitation at the top and bottom of the copper pads. Finally, there could be a combination of the two explanations.

*TABLE 2. SOLDER BALL GEOMETRY PARAMETERS.*

| **Parameter** | **Standoff Height (mils)** | **Radius (mils)** | **Pitch (mils)** | **Array** |
|---|---|---|---|---|
| **Value** | 20.5 | 15.8 | 60 | 2x2 |

*TABLE 3. COMPARISON OF CALCULATION, SIMULATION, AND MEASUREMENT FOR A 4X4 SBA.*

| **Method** | **Inductance (@ 1.25 GHz)** |
|---|---|
| Calculation | 30.2 pH |
| Simulation | 34.3 pH |
| Measurement | 1.3 nH |

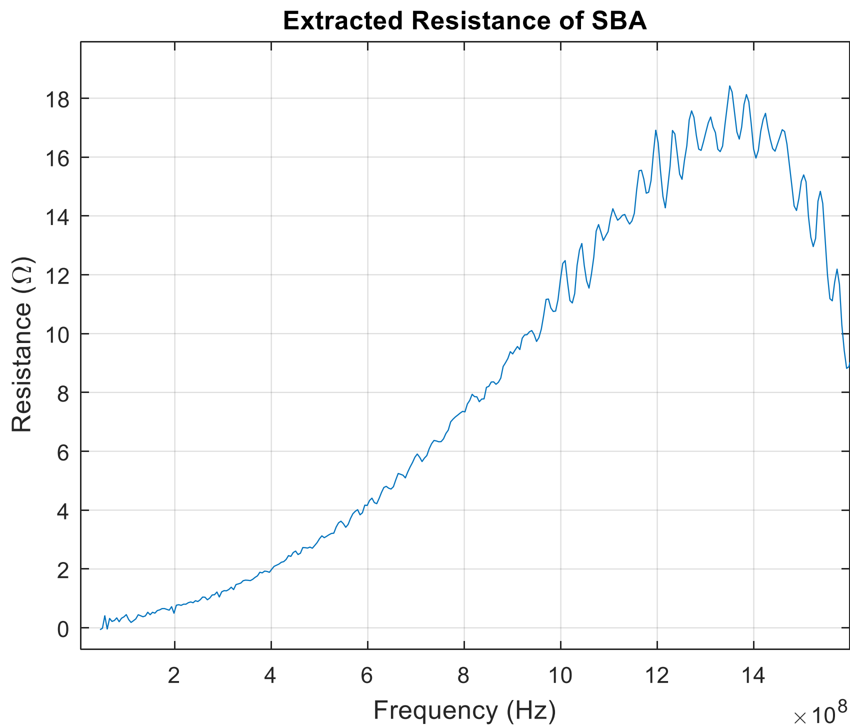


*Figure 27. Resistance measurement for valid frequency range.*

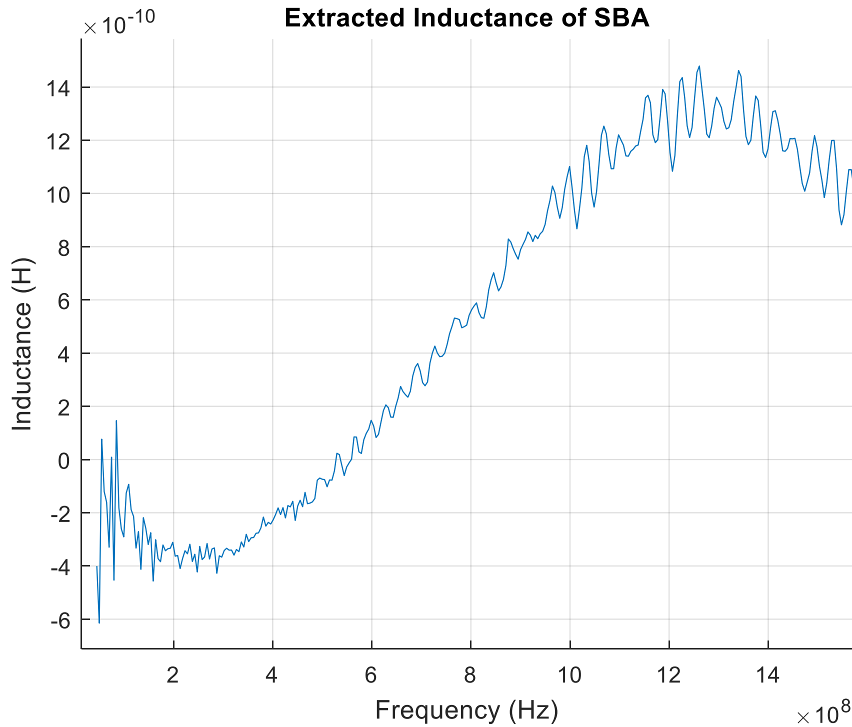


***Figure 28. Inductance measurement for valid frequency range.***

## VI. Future Work

This work focuses on the inductance of solder balls and solder ball arrays with some attention given to their resistance with frequency; however, the impedance profile of SBAs is incomplete. Explorations into capacitance of the arrays is needed to fully realize a complete model. Adding calculated capacitance into the model would benefit software such as PowerSynth and would inform evaluations of measured data. Zhang and Fan [18] provide a lumped capacitance model that may be useful in completing a future RLC model similar to work by Jin et al. [19].

As discussed earlier, the experimental data is not sufficient to validate the proposed characterization methods. More work may be done to refine the test fixtures and procedures such that the measured data is more insightful. This work includes fabrication of test fixtures by reputable PCB manufacturers to cut

down inconsistencies caused by the CNC milling machine, refining the fixture layout to emulate power module excitation of SBAs, and measuring open fixtures before attachment by reflowed solder balls.

## VII. CONCLUSIONS

The mathematical models established in this paper to predict the inductance of reflowed solder balls and SBAs are validated by FEA performed in ANSYS Electromagnetics Suite, but not by experimental data. According to simulation data, a cylindrical short wire formula will reliably approximate a single, ideal, reflowed solder ball. Likewise, the formula for mutual inductance of two cylindrical wires is sufficient to approximate the magnetic coupling between two interconnects in a SBA. These calculated values can then be used to solve a network of interconnects for total inductance using matrix operations. The result of total array inductance error is approximately 20% across all distances for values in the picoHenry range.

This method of finding parasitic inductance for 3D architectures is well suited for implementation into software platforms such as PowerSynth. The characterization model may be improved with an additional capacitance parameter. More effort into experimental validation of the model is necessary. Future testing of real modules with identical 3D architectures will be useful in refining the models presented in this paper.

## VIII. REFERENCES


[1] A. S. Bahman, F. Blaabjerg, A. Dutta and A. Mantooth, "Electrical parasitics and thermal modeling for optimized layout design of high power SiC modules," *2016 IEEE Applied Power Electronics Conference and Exposition (APEC),* pp. 3012-3019, 2016.

[2] Q. Le, S. Mukherjee, T. Vrotsos and H. A. Mantooth, "Fast transient thermal and power dissipation modeling for multi-chip power modules: A preliminary assessment of different electro-thermal evaluation methods," *2016 IEEE 17th Workshop on Control and Modeling for Power Electronics (COMPEL),* pp. 1-6, 2016.

[3] T. M. Evans and e. al., "PowerSynth: A Power Module Layout Generation Tool," *IEEE Transactions on Power Electronics.*

[4] F. Yang, Z. Liang, Z. Wang and F. Wang, "Parasitic inductance extraction and verification for 3D Planar Bond All Module," in *2016 International Symposium on 3D Power Electronics Integration and Manufacturing (3D-PEIM)*, Raleigh, NC, 2016.

[5] S. Seal, M. D. Glover and H. A. Mantooth, "3-D Wire Bondless Switching Cell Using Flip-Chip-Bonded Silicon Carbide Power Devices," *IEEE Transactions on Power Electronics,* vol. 33, no. 10, pp. 8553-8564, Oct. 2018.

[6] A. Boyer, E. Sicard, M. Fer and L. Courau, "Electrical characterization of a 64 Ball Grid Array package," in *2008 International Symposium on Electromagnetic Compatibility - EMC*, Europe, Hamburg, 2008.

[7] T.-S. Horng, S.-M. Wu, A. Tseng and H.-H. Huang, "Electrical modelling of enhanced ball grid array packages using coupled transmission lines," *Electronics Letters,* vol. 35, no. 18, pp. 1567-1569, 2 Sept. 1999.

[8] C.-T. Peng, C.-M. Liu, J.-C. Lin, H.-C. Cheng and K.-N. Chiang, "Reliability analysis and design for the fine-pitch flip chip BGA packaging," *IEEE Transactions on Components and Packaging Technologies,* vol. 27, no. 4, pp. 684-693, Dec. 2004.

[9] C.-A. Yuan and K.-N. Chiang, "An overview of solder bump shape prediction algorithms with validations," *IEEE Transactions on Advanced Packaging, vol. 24, no. 2,* pp. 158-162, May 2001.

[10] H. A. Aebischer and B. Aebischer, "Improved Formulae for the Inductance of Straight Wires," *Advanced Electromagnetics,* vol. 3, no. 1, p. 31, Aug. 2014.

[11] J. Jeong and J. Jeong, "Electrical characterization of ball grid array packages from S-parameter measurements below 500 MHz," in *IEEE 7th Topical Meeting on Electrical Performance of Electronic Packaging*, West Point, NY, USA, 1998.

[12] O. M. O. Gatous and J. Pissolato, "Frequency-dependent skin-effect formulation for resistance and internal inductance of a solid cylindrical conductor," *IEEE Proceedings - Microwaves, Antennas and Propagation,* vol. 151, no. 3, pp. 212-216, 21 June 2004.

[13] J. W. Nilsson and S. A. Riedel, Electric circuits, Hoboken, NJ: Pearson Education, Inc., 2019.

[14] R. W. Anderson, "S-Parameter Techniques for Faster, More Accurate Network Design," Hewlett Packard, 1967.

[15] T. Reveyrand, "Multiport conversions between S, Z, Y, h, ABCD, and T parameters," in *2018 International Workshop on Integrated Nonlinear Microwave and Millimetre-wave Circuits (INMMIC)*, Brive La Gaillarde, France, 2018.

[16] D. A. Frickey, "Conversions between S, Z, Y, H, ABCD, and T parameters which are valid for complex source and load impedances," *IEEE Transactions on Microwave Theory and Techniques,* vol. 42, no. 2, pp. 205-211, 1994.

[17] MathWorks, "Convert S-parameters to Y-parameters - MATLAB s2y," [Online]. Available: https://www.mathworks.com/help/rf/ug/s2y.html. [Accessed 23 April 2019].

[18] Y. Zhang and J. Fan, "An Intrinsic Circuit Model for Multiple Vias in an Irregular Plate Pair Through Rigorous Electromagnetic Analysis," *IEEE Transactions on Microwave Theory and Techniques,* vol. 58, no. 8, pp. 2251-2265, Aug. 2010.

[19] S. Jin, et and al., "Analytical Equivalent Circuit Modeling for BGA in High-Speed Package," *IEEE Transactions on Electromagnetic Compatibility,* vol. 60, no. 1, pp. 68-76,, Feb. 2018.